((Catch Phrase))

DOI: 10.1002/anie.200((will be filled in by the editorial staff))

Nano-sized Au@Prussian Blue Analogues Heterostructures: Towards Multifunctionality at the Nanoscale.**

Guillaume Maurin-Pasturel, Jérôme Long, Yannick Guari, Franck Godiard, Marc-Georg Willinger, Christian Guerin and Joulia Larionova*

((Dedication----optional))

Coordination polymer nanoparticles (NPs) are intriguing molecule-based nano-sized materials, made of metal ion nodes and molecular building blocks, which attract a great deal of attention during the last decade. Such interest is firstly due to many of specific features originating from their intrinsic molecular nature such as determined and flexible molecular structures, porosity, low density, tuneable physical and chemical properties, and "soft" chemistry routes for their synthesis.[1] Moreover, due to the high surface-to-volume atomic ratio, they possess unique size- and shape-dependent electrical, optical, magnetic, and catalytic properties that are strikingly different from their bulk counterparts. Different families of nano-sized molecule-based materials including Metal Organic Frameworks (MOFs),[2] infinite coordination polymers[3] or cyano-bridged coordination polymers also known as Prussian Blue and its analogues (PBA)[4] have recently been investigated.

A new focus of the research activity on coordination polymers at the nanoscale, in addition of being a new synthetic challenge, is to combine them with other materials into core@shell heterostructures. The design of such intricate materials, where the different chemical composition meet at interface constitutes a promising way towards multifunctional nanomaterials combining multiple properties in a single system and exhibiting diverse physical responses when subjected to various external stimuli.[5] The heterostructures can either present simple coexistence of physical and chemical properties of the constitutive components or display novel ones due to the mutual interaction between the core and shell components. Numerous examples of inorganic core@shell nanoparticles (NPs) associating various properties or improving the existent ones have previously been reported.[6] We can cite semiconductor@semiconductor[7] and metal@semiconducteur nanocrystals[8] with tuned optical properties, metal@metal,[9] metal@metal oxide, metal oxide@metal nano-objects with advanced catalytic, optical, magneto-plasmonic properties,[10] and metal or metal oxide@silica NPs, which have been proposed as multifunctional platforms for a variety of applications.[11] On the other hand, examples of heterostructures where one of whose components is a coordination polymer remain relatively scarce. Several heterostructurated systems combining inorganic materials with coordination polymers or MOFs were investigated for their enhanced catalytic activity or for an association of the magnetic or optical properties of inorganic NPs with porosity, electrochemical or magnetic properties of the coordination polymers.[5], [12]-[14] In most cases, multiple metal (Au, Pt, Ag, Pd, Ru, Cu, Ni),[12] metal oxide (Fe_3O_4)[13] or quantum dots (CdTe, ZnO) NPs[14] were embedded in various porous MOFs matrixes to give micro- or nano-sized hybrid systems. Among these inorganic cores, gold NPs are particularly appropriate to design multifunctional systems thanks to the catalytic properties and the optical properties arising from the surface Plasmon band. Concerning Au-core containing nano-heterostructures, we can cite MOF (with MOF = $Zn_4O(BDC)_3$, BDC=1,4-benzenedicarboxylate) decorated gold NPs presenting selectivity for CO_2 entrapment,[15] Au NPs encapsulated by MIL-100(Fe) [16] or by ZIF-8 (Zn^{2+}-based imidazolate framework)

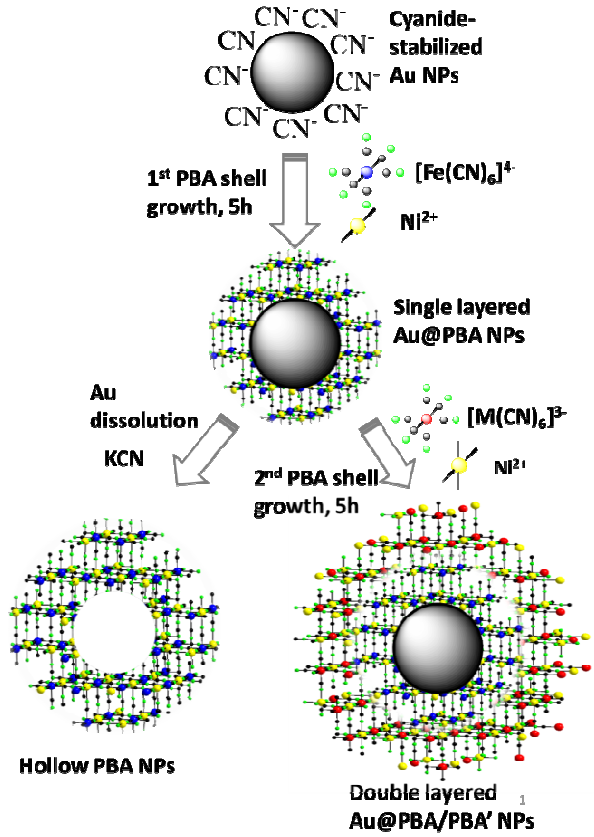

Figure 1. Schematic representation of single Au@PBA and double layered Au@PBA@PBA' core-shell NPs as well as hollow PBA NPs obtained through the cyano-bridged coordination network growth on the Au surface.

[*] G. Maurin-Pasturel, Dr. J. Long, Dr. Y. Guari, Prof. Dr. C. Guérin, Prof. Dr. J. Larionova
Institut Charles Gerhardt Montpellier, UMR 5253 CNRS-UM2-ENSCM-UM1
Equipe Chimie Moléculaire et Organisation du Solide
Université Montpellier 2, Place Eugène Bataillon, 34095 Montpellier Cedex 5, France.
Fax: (+) 33 4 67 14 38 52
E-mail: yannick.guari@um2.fr
F. Godiard
Service de microscopie électronique, Université Montpellier 2, Place Eugène Bataillon, 34095 Montpellier Cedex 5, France
Dr. M.-G. Willinger
Fritz Haber Institute of the Max Planck Society, Department of Inorganic Chemistry, Faradayweg 4-6, D-14195 Berlin, Germany

[**] The authors are grateful to UM2, CNRS, PAC ICGM.

Supporting information for this article is available on the WWW under http://www.angewandte.org or from the author.((Please delete if not appropriate))

shell[17] presenting enhanced catalytic activity *via* a synergic effect. However, to the best of our knowledge, no report has been devoted to the design of core@shell heterostructures where a single inorganic NP was coated by a uniform and well defined layer of coordination polymer to give strictly individual core-shell heterostructures at the nanoscale. In the present manuscript we report a new and a rational approach for the design of single and double layered multifunctional magneto-optical Au@PBA heterostructures of uniform shape having tuneable thickness of the coordination polymer shell and exhibiting the characteristic surface Plasmon band of gold core and magnetic properties of PBA shell. Remarkably, the gold core can be post-synthetically removed to give hollow PBA nano-structures.

The single layered Au@PBA heterostructures were obtained by a two-step approach (Fig. 1, see ESI for Experimental Part) consisting of: (*i*) the synthesis of cyanide-stabilised gold NPs in water by reduction of the dicyanoaurate precursor $[Au(CN)_2]^-$ by potassium borohydride,[18] and (*ii*) the subsequent time-controlled growth of the cyano-bridged coordination polymer shell on the surface of these gold NPs. The reaction between $[Au(CN)_2]^-$ and KBH_4 in water yields to the appearance of a characteristic red colour indicating the formation of gold NPs. After 20 min. of reaction, the cyano-bridged coordination shell can be grown by the simultaneous addition of two aqueous solutions of the respective molecular precursors, $K_3[Fe^{III}(CN)_6]$ and $Ni^{II}Cl_2{\cdot}6H_2O$. The precursors' addition rate control (2 mL/hour) is essential to foster growth of the cyano-bridged network preferentially at the surface of gold NPs over a self-nucleation. After complete addition (5 hrs), the obtained single layered $Au@KNi^{II}[Fe^{II}(CN)_6]$ (Au@KNiFe) NPs were recovered by centrifugation and washed with water and ethanol. Their Infra-Red (IR) spectra confirms the formation of the cyano-bridged network, with a broad single band at 2094 cm^{-1} in the cyanide stretching region, characteristic of the Fe^{II}-CN-Ni^{II} (Fig. 1S, ESI).[19] It clearly indicates a reduction of the $[Fe^{III}(CN)_6]^{3-}$ cyanometallate moiety into $[Fe^{II}(CN)_6]^{4-}$ during the growing shell process due to the presence of borohydride. Elemental analysis allows to determine the NPs' composition of $Au_{1.08}@K_{1.20}Ni^{II}[Fe^{II}(CN)_6]_{0.80}$. Magnetic measurements support the total reduction of the cyanometallate moiety showing that the Au@KNiFe NPs behave as a paramagnetic compound with interactions between Ni^{2+} ions through the diamagnetic $[Fe^{II}(CN)_6]^{4-}$ moiety at low temperature (Fig. 2S, ESI).

Powder X-Ray Diffraction (PXRD) pattern further confirms the formation of the targeted heterostructure (Fig. 3S). Diffraction peaks characteristic of the *fcc* gold metal structure (00-004-0784) are observed at 38.2, 44.4, 64.7 and 77.7 ° and are indexed in the space group *Fm-3m* with a cell parameter a_{gold} = 4.08 Å. The crystalline domain was calculated from the Scherrer formula giving an average value of *ca.* 15 nm. In addition, the PXRD pattern exhibits characteristic peaks of the *fcc* structure of $Ni^{II}_2[Fe^{II}(CN)_6]$ indexed in the *F4-3m* (01-075-0037) space group with a cell parameter of a_{NiFe} = 10.07 Å and a crystalline domain size of *ca.* 26 nm (d_{200} reflection).

Transmission Electronic Microscopy (TEM) and High Resolution Transmission Electronic Microscopy (HRTEM) measurements show that the obtained NPs present well defined core@shell structures with a uniform size and shape (Fig. 2 and Fig. 4S, ESI). The gold cores have a mean diameter of 19.5 ± 4.3 nm, which is consistent with the value obtained from PXRD. Each single core is coated by a coordination polymer shell to result in core@shell NPs with a whole diameter of 52.4 ± 8.6 nm. Selected Area Electron Diffraction on individual nanoparticles confirms the presence of both Au and $K_{1.20}Ni^{II}[Fe^{II}(CN)_6]_{0.80}$ crystalline phases (Fig 5S, ESI).

In order to demonstrate the shell growing mechanism on the Au surface, the $K_{1.20}Ni^{II}[Fe^{II}(CN)_6]_{0.80}$ shell formation was followed in time by TEM observation. A series of TEM images taken during the PBA shell growth shows a regular increase of the size thickness for a reaction time ranging from 20 mins to 5 hrs (Figs. 6S & 7S, ESI). Note that the size of the Au core remains the same during the shell growth. It is therefore reasonable to presume that the formation of the PBA shell occurs *via* the coordination of the Ni^{2+} and/or ferrocyanide moieties on the gold surface at the beginning of the growth process rather that during a post-synthetic redistribution of the negatively charged PBA NPs at the gold surface. Note also that performing the same reaction with $HAuCl_4$ as gold precursor does not yield to the targeted heterostructures indicating the decisive role of cyanides to direct the growth of the PBA shell.

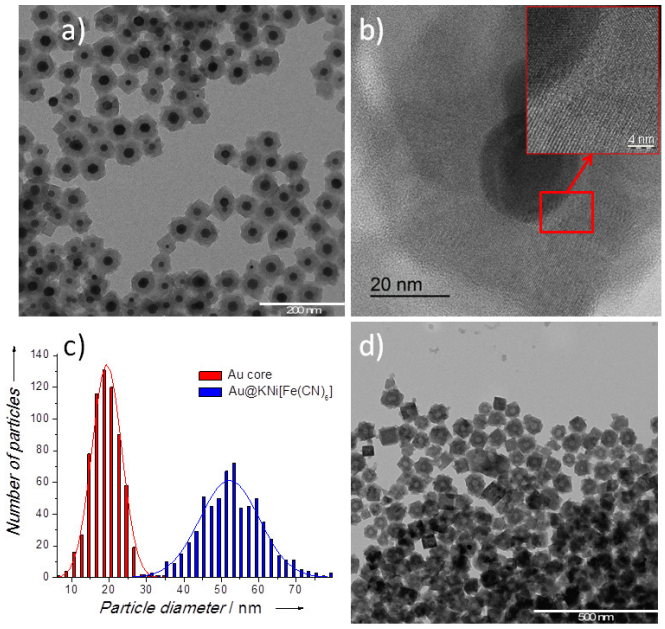

Figure 2. TEM (a) and HRTEM (b) images of the Au@KNiFe NPs; c) corresponding histograms of the size distribution for the gold core (red) and the total size (blue); d) TEM image of the hollow $KNi[Fe(CN)_6]$ NPs.

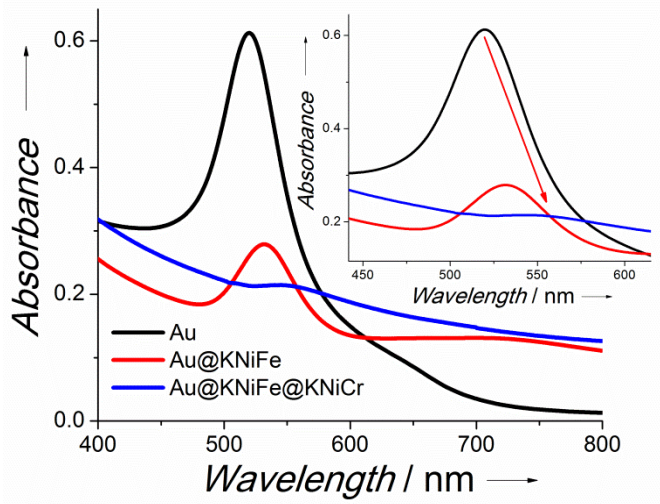

Figure 3. Electronic spectra of Au, Au@KNiFe, Au@KNiFe@KNiCr NPs in the visible region. Inset: magnification of the gold surface Plasmon band region.

The optical properties of uncoated gold NPs exhibit an intense surface plasmon absorption band in the visible region at 520 nm (Fig. 3).[20] The exact position and width of this band are extremely

sensitive to any perturbation of the gold surface[21] and, by extension, to the presence of a PBA shell. The refractive index of the cyano-bridged coordination polymer shell is different from that of the gold and the surrounding water. As the gold NPs are covered with $K_{1.20}Ni^{II}[Fe^{II}(CN)_6]_{0.80}$, the surface plasmon band is red-shifted to λ_{max} = 533 nm (Fig. 3), as predicted by the Mie theory and observed in the case of gold NPs coated with a relatively thin (< 60 nm) layer of silica,[22] ZrO_2 or TiO_2.[23] This is explained by an increase in the local refractive index around the gold NPs.

It is well known that due to the high stability constant of the gold cyanide complex $[Au(CN)_2]^-$ (10^{37} M^{-2}),[24] the gold NPs are subject to an etching process in the presence of cyanide and oxygen. Thanks to the intrinsic porosity of the PBA network, hollow PBA NPs can be obtained by simple dispersion of the core-shell Au@KNiFe NPs in a 10^{-3} M KCN solution (Fig. 1). This reaction induces the disappearance of the red colour indicating a dissolution of the gold cores through the pores of the PBA shell with formation of the colourless PBA hollow NPs and gold cyanide complex $[Au(CN)_2]^-$ in solution.[18] The etching reaction was followed by electronic spectroscopy showing the vanishing of the surface Plasmon band after 23 h indicating the complete core dissolution (Fig. 8S). The integrity of the $K_{1.20}Ni^{II}[Fe^{II}(CN)_6]_{0.80}$ cyano-bridged network of the isolated hollow NPs was attested by IR spectroscopy showing the presence of the characteristic band at 2094 cm^{-1} (Fig. 9S). TEM analysis of these NPs revealed the formation of hollow nano-objects with a mean size of 53.8 ± 5.2 nm, closed to the size of the initial core@shell NPs (Fig. 2d).

The multifunctional double layered Au@PBA@PBA' heterostructures presenting both plasmonic and magnetic properties may be obtained from the single layered Au@PBA NPs by growing a second ferromagnetic magnetic shell. Note that the possibility of epitaxial growth surface of a cyano-bridged coordination polymer at the surface of another cyano-bridged coordination polymer with closed cell parameters has already been demonstrated by using surfactant free core NPs.[25] In this line of thought, the single layer Au@KNiFe NPs were further reacted with $K_3[Cr^{III}(CN)_6]$ and $Ni^{II}Cl_2{\cdot}6H_2O$ reagents in the same conditions as those which led to the formation of the first shell for the design of $Au@KNi^{II}[Fe^{II}(CN)_6]@KNi^{II}[Cr^{III}(CN)_6]$ (Au@KNiFe@KNiCr) NPs (Fig. 1). IR spectroscopy indicates the appearance of an additional Cr(III)-CN-Ni(II) bridging stretching vibration at 2172 cm^{-1} besides the cyanide stretching vibration at 2090 cm^{-1} characteristic of the first Fe(II)-CN-Ni(II) layer (Fig. 10S). The PXRD pattern also shows two sets of distinct peaks confirming the presence of $KNi^{II}[Fe^{II}(CN)_6]$ and $KNi^{II}[Cr^{III}(CN)_6]$ shells in accordance to the significant difference of the relative cell parameters determined as a_{NiCr} = 10.46 Å and a_{NiFe} = 10.07 Å (Fig. 3S). TEM observations confirm the subsequent growth of a second PBA shell (Fig. 11S) showing the presence of the uniform in size and shape NPs with a gold core mean size of 20.6 ± 3.2 nm and an average diameter size of 133.3 ± 11.5 nm. EDS mapping was carried out to confirm the growth of the second layer (Fig. 4). Figure 4d shows the distribution of iron (red) and of chromium (green), the latter being present in the second layer at the periphery of the NPs indicating that no redistribution and mixing of the PBA phases occurs between the different layers during the growth process.

The double layered Au@KNiFe@KNiCr NPs present both the plasmonic properties of the gold core and the magnetic properties of the second cyano-bridged coordination polymer shell. The surface plasmon band is shifted to higher wavelength (red shift) (λ_{max} = 545 nm) in comparison with the single-shell NPs (Fig. 3), which is consistent with the increase of the shell thickness.[22] The presence of the second PBA shell induces the enlargement of the plasmon band, which may be explained by the confinement of the free electrons within the metal core.[23]

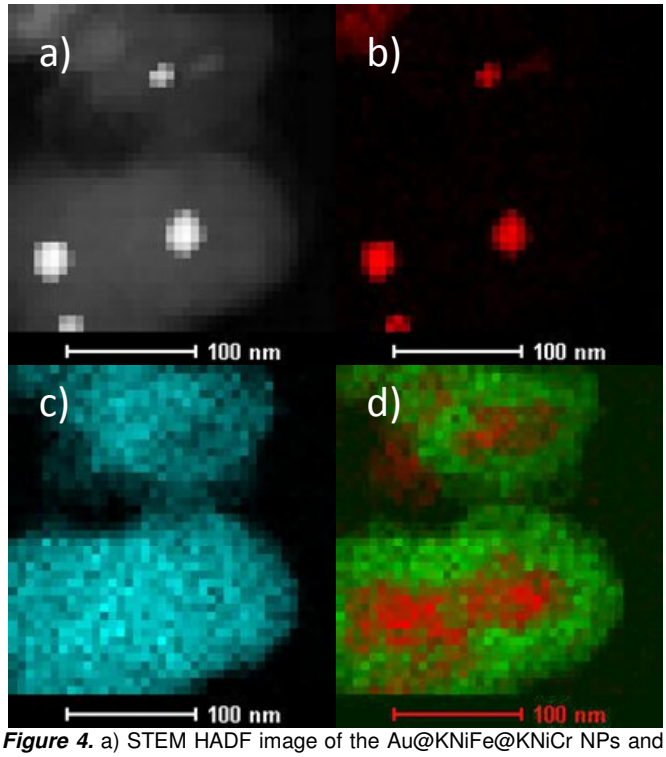

Figure 4. a) STEM HADF image of the Au@KNiFe@KNiCr NPs and the corresponding EDS mapping for b) gold (red), c) nickel (blue) and d) iron (red) and chromium (green).

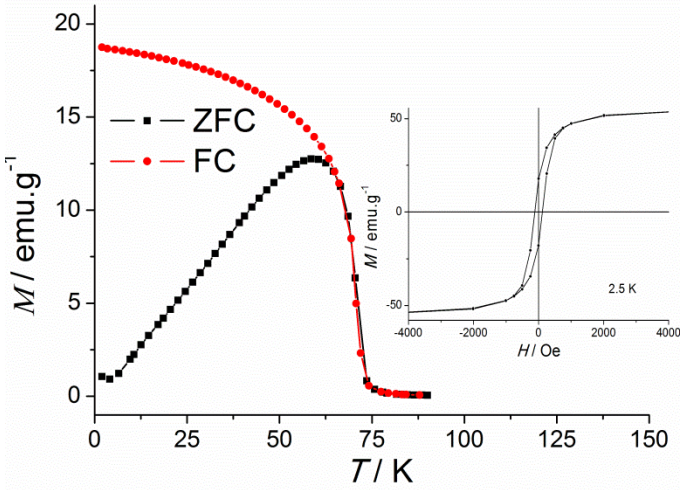

Figure 5. ZFC/FC magnetization curves performed for Au@KNiFe@KNiCr with an applied field of 100 Oe. Inset: hysteresis loop performed at 2.5 K.

The magnetic properties of Au@KNiFe@KNiCr were performed using a SQUID-MPMS magnetometer working in the temperature range 1.8 – 350 K up to 7 T firstly by applying the Zero Field-Cooled (ZFC)-Field Cooled (FC) magnetization protocol (Fig. 5). The ZFC curve exhibits a peak with a maximum at 60 K, corresponding to the blocking temperature of the mean size NPs, while the FC curve increases as the temperature decreases. The ZFC/FC curves start to diverge below 65 K, indicating a relatively narrow size distribution of the NPs. The field dependence of the magnetization measured at 2.5 K shows the presence of a small hysteresis effect with a coercive field of 110 Oe confirming the blocking of the magnetization. Both values of the blocking temperature and the coercive field are in accordance with the values

previously obtained for $ANi[Cr(CN)_6]$ NPs (A: alkaline cation) with a size larger than 20 nm.[26]

In summary, the described rational approach consisting of the growth of a cyano-bridged coordination polymer at the surface of gold NPs appears promising for the design of core@shell nano-heterostructures with a single or multiple PBA shells as well as for the generation of hollow PBA nano-objects. The former presents well-defined core@shell structures with a single gold core and a single PBA shell in close interaction and constitutes the first example of such hybrid heterostructure involving PBA. They combine plasmonic optical properties of the gold core and magnetic properties of the PBA shell with a paramagnetism in the case of single layer and a ferromagnetism for double layer nanostructures and may be, consequently, considered as multifunctional. Moreover, the composition of the coordination polymer shell can be easily tailored by changing the metal ions that induces a change of the magnetic properties. The extension of the simple synthetic procedure presented in this article to other nanoscale heterostrures with various cyano-bridged coordination polymers with magnetic, host guest or optical properties opens new perspectives toward the design of multifunctional nano-systems involving coordination polymers.

Received: ((will be filled in by the editorial staff))
Published online on ((will be filled in by the editorial staff))

Keywords: gold nanoparticles · Prussian Blue nanoparticles · core-shell · coordination networks · magnetic properties

[1] M. Oh, C. A. Mirkin, *Nature* **2005**, *438*, 651;

[2] a) P. Horcajada, R. Gref, T. Baati, P. K. Allan, G. Maurin, P. Couvreur, G. Férey, R. E. Morris, Ch. Serre, *Chem. Rev*., **2012**, *112*, 1232; b) K. M. L. Taylor, A. Jin, W. Lin, *Angew. Chem. Int. Ed.* **2008**, *47*, 7722.

[3] A. M. Spokoyny, D. Kim, A. Sumrein, C. A. Mirkin, *Chem. Soc. Rev.*, **2009**, *38*, 1218.

[4] a) J. Larionova, Y. Guari, C. Sangregorio, C. Guérin, *New J. Chem.* **2009**, *33*, 1177; b) L. Catala, F. Volatron, D. Brinzei, T. Mallah, *Inorg. Chem.* **2009**, *48*, 3360; c) E. Dujardin, S. Mann, *Adv. Mater.* **2004**, *16*, 1125.

[5] S. B. Kim, C. Cai, S. Sun, D. A. Sweigart, *Angew. Chem.* **2009**, *121*, 2951; *Angew. Chem. Int. Ed*. **2009**, *48*, 2907; b) H.-L. Jiang, B. Liu, T. Akita, M. Haruta, H. Sakurai, Q. Xu, *J. Am. Chem. Soc.* **2009**, *131*, 11302; c) J. Son, H. J. Lee, M. Oh, *Chem. Eur. J*. **2013**, 19, 6546; d) S. Hermes, M.-K. Schrecter, R. Schmid, L. Khodeir, M. Muhler, A. Tissler, R. W. Fischer, R. A. Fischer, *Angew. Chem.* **2005**, *117*, 6394; *Angew. Chem. Int. Ed*. **2005**, *44*, 6237; e) H. J. Lee, W. Cho, M. Oh, *Chem. Commun*. **2012**, *48*, 221; f) C. Jo, H. J. Lee, M. Oh, *Adv. Mater*. **2011**, *23*, 1716 .

[6] R. Ghosh Chaudhuri, S. Paria, *Chem. Rev*., **2012**, *112*, 2373.

[7] for instance (a) P. Reiss, M. Protière, L. Li, *Small*, **2009**, *5*, 154; b) Y. W. Cao, U. Banin, *J. Am. Chem. Soc*. **2000**, *122*, 9692; c) J. Wang, H. J. Han, *Colloid Interface Sci*. **2010**, *351*, 83; d) X. Peng, M. C. Schlamp, A. V. Kadavanich, A. P. Alivisatos, *J. Am. Chem. Soc.* **1997**, *119*, 7019; e) G. G. Yordanov, H. Yoshimura, C. D. Dushkin, *Colloid. Polym. Sci.* **2008**, *286*, 1097.

[8] a) R. Costi, A. E. Saunders, U. Banin, *Angew. Chem., Int. Ed.* **2010**, *49*, 4878; b) J. T .hang, Y. Tang, K. Lee, M. Ouyang, *Science* 2010, 327, 1634; c) Y. Lei, W.-K. Chim, *J. Am. Chem. Soc.* **2005**, 127, 1487; d) L. Zhang, D. A. Blom, H. Wang *Chem. Mater.* **2011**, *23*, 4587; e) C. Gu, M. Park, C. Shannon *Langmuir*, **2009**, *25*, 410; f) Z. Sun, Z. Yang, J. Zhou, M. H.Yeung, W. H. Ni, H. Wu, J. F. Wang, *Angew. Chem., Int. Ed.* **2009**, 48 , 2881.

[9] for instance: a) Y. W. Lee, M. Kim, Z. H. Kim, S. W. Han, *J. Am. Chem. Soc.* **2009**, *131*, 17036; b) F. Bao, J. F. Li, B. Ren, J. L.Yao, R. A. Gu, Z. Q. Tian, *J. Phys. Chem. C* **2008**, *112*, 345; c) X. B. Zhang, J. M. Yan, S. Han, H. Shioyama, Q. Xu, *J. Am. Chem. Soc.* **2009**, *131*, 2778; d) W. R. Lee, M. G. Kim, J. R. Choi, J.-I. Park, S. J. Ko, S. J. Oh, J. Cheon *J. Am. Chem. Soc.* **2005**, *127*, 16090; e) C. Gu, H. Xu,; M. Park, C. Shannon *Langmuir* **2009**, *25,* 410; f) J.-W. Hu, J.-F. Li, B. Ren, D.-Y. Wu, S.-G. Sun, Z.-Q. Tian *J. Phys. Chem. C* **2007**, *111*, 1105.

[10] for instance: a) W. Shi, H. Zeng, Y. Sahoo, T. Y. Ohulchanskyy, Y. Ding, Z. L. Wang, P. N. Prasad, *Nano Lett.* **2006**, *6*, 875; b) F. Pineider, C. de Julian Fernandez, V. Videtta, E. Carlino, A. al Hourani, F. Wilhelm, A. Rogalev, P. D. Cozzoli, P. Ghigna, C. Sangregorio, *ACS Nano*, **2013**, *7*, 857; c), K. C.-F. Leung, S. Xuan, X. Zhu, D. Wang, C.-P. Chak, S.-F. Lee, W. K.-W. Ho, B. C.-T. Chung, *Chem. Soc. Rev.* **2012**, *41*, 1911; d) Y. Yin, R. M. Rioux, C. K. Erdonmez, S. Hughes, G. A. Somorjai, A. P. Alivisatos, *Science* **2004**, *304*, 711; e) C. Levin, C. Hofmann, T. A. Ali, A. T. Kelly, E. Morosan, P. Nordlander, K. H. Whitmire, N. J. Halas, *ACS Nano* **2009**, *3*, 1379

[11] for instance a) F.Mazaleyrat, M. Ammar, M. LoBue, J. P. Bonnet, P. Audebert, G. Y. Wang, Y. Champion, M. Hytch, E. J. Snoeck, *Alloys Compd.* **2009**, *483*, 473; b) J. Lee, Y. Lee, J. K. Youn, H. B. Na, T. Yu, H. Kim, S. M. Lee, Y. M. Koo, J. H. Kwak, H. Park, H. N. Chang, M. Hwang, J. G. Park, J. Kim, T. Hyeon, *Small* **2008**, *4,* 143; c) F. G. Aliev, M. A. Correa-Duarte, A. Mamedov, J. W. Ostrander, M. Giersig, L. M. Liz-Marzan, N. A. Kotov *Adv. Mater.* **1999**, *11*, 1006; d) F. Mazaleyrat, M. Ammar, M. LoBue, J. P. Bonnet, P. Audebert, G.Y. Wang, Y. Champion, M. Hytch, E. J. Snoeck, *Alloys Compd.* **2009**, *483*, 473.

[12] a) J.-D. Qiu, H.-Z. Peng, R.-P. Liang, J. Li, X.-H. Xia, *Langmuir.* **2007**, *23*, 2133 ; b) K. Liu, R. Yuan, Y. Chai, D. Tang, H. An, *Bioprocess. Biosyst Eng.* **2010**, *33*, 179; c) Z. Chu, Y. Zhang, X. Dong, W. Jin, N. Xu, B. Tieke, *J. Mater. Chem.* **2010**, *20*, 7815; d) C. Wang, S. Chen, Y. Xiang, W. Li, X. Zhong, X. Che, J. Li, *J. Mol. Catal. B: Enzym* **2011**, *69*, 1; e) Y. Namiki, T. Namiki, Y. Ishii, S. Koido, Y. Nagase, A. Tsubota, N. Tada, Y. Katamoto, *Pharm. Res.* **2012**, *29*, 1404 ; f); L. Jin, Y. Fang, L. Shang, Y. Liu, J. Li; L. Wang, P. Hu, S. Dong, *Chem. Commun.* **2013**, *49*, 243.

[13] F. Ke, L.-G. Qiu, Y.-P. Yuan, X. Jiang, J.-F. Zhu, *J. Mater. Chem.* **2012**, *22,* 9497.

[14] a) P. L. Feng, J. J. Perry IV, S. Nikodemski, B. W. Jacobs, S. T. Meek, M. D. Alledorf, *J. Am. Chem. Soc*. **2010**, *132*, 15487.

[15] L. He, Y. Liu, J. Liu, Y. Xiong, J. Zheng, Y. Liu, Z. Tang, *Angew. Chem. Int. Ed*. **2013**, *52*, 3741 – 3745;

[16] F. Ke, J. Zhu, L.-G. Qiu, X. Jiang, *Chem. Commun.* **2013**, *49*, 1267.

[17] G. Lu, S. Z. Li, Z. Guo, O. K. Farha, B. G. Hauser, X. Y. Qi, Y. Wang, X. Wang, S. Y. Han, X. G. Liu, J. S. DuChene, H. Zhang, Q. C. Zhang, X. D. Chen, J. Ma, S. C. J. Loo, W. D. Wei, Y. H. Yang, J. T. Hupp, F. W. Huo, *Nature Chem*., **2012**, *4*, 310.

[18] C.-C. Huang, W.-C. Lai, C.-Y. Tsai, C.-H. Yang, C.-S. Yeh, *Chem. Eur. J*. **2012**, *18*, 4107.

[19] a) O. Sato, *J. Solid. State Electrochem.*, **2007**, *11*, 773; b) O. N. Risset, E. S. Knwoles, S. Ma, M. W. Meisel, D. R. Talham, *Chem. Mater.* **2013**, *25*, 42.

[20] See for instance: C. J. Murphy, A. M. Gole, S. E. Hunyadi, C. J. Orendorff, *Inorg. Chem.* **2006**, *45*, 7544.

[21] K. M. Mayer, J. H. Hafner, *Chem. Rev.* **2011**, *111*, 3828.

[22] L. M. Liz-Marzan, M. Giersig, P. Mulvaney, *Langmuir*, **1996**, *12*, 4329 .

[23] R. T. Tom, A. Sreekumaran Nair, N. Singh, M. Aslam, C. L. Nagendra, R. Philip, K. Vijayamohanan, T. Pradeep, *Langmuir*, **2003**, *19*, 3439 .

[24] M. A. Rawashdeh-Omary, M. A. Omary, H. H. Patterson, *J. Am. Chem. Soc.* **2000**, *122*, 10371.

[25] a) D. Asakura, C. H. Li, Y. Mizuno, M. Okubo, H. Zhou, D. R. Talham, *J. Am. Chem. Soc.*, **2013**, *135*, 2793; b) M. F. Dumont, E. S. Knowles, A. Guiet, D. M. Pajerowski, A. Gomez, S. W. Kycia, M. W. Meisel, D. R. Talham, *Inorg. Chem.* **2011**, *50*, 4295; c) L. Catala, D. Brinzei, Y. Prado, A. Gloter, O. Stéphan, G. Rogez, T. Mallah, *Angew. Chem. Int. Ed.*, **2009**, *48*, 183; d) Y. Prado, N. Dia, L. Lisnard, G. Rogez, F. Brisset, L. Catala, T. Mallah, *Chem. Commun.* **2012**, *48*, 11455; e) M. Presle, J. Lemainque, J.-M. Guigner, E. Larquet, I. Maurin, J.-P. Boilot, T. Gacoin, *New J. Chem.* **2011**, *35*, 1296.

[26] Y. Prado, L. Lisnard, D. Heurtaux, G. Rogez; A. Gloter, O. Stéphan, N. Dia, E. Rivière, L. Catala, T. Mallah, *Chem. Commun.* **2011**, *47*, 1051.

Entry for the Table of Contents (Please choose one layout)

Layout 1:

((Catch Phrase))

((Author(s), Corresponding Author(s)*))
_____ **Page – Page**

((Title Text))

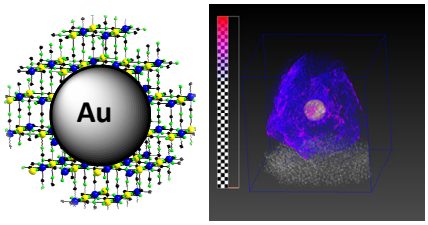

The single and double layered core-shell heterostructures based on well-defined gold core and Prussian Blue analogous shells present magneto-optical properties and maybe considered as multifunctional nano-objects.

Layout 2:

((Catch Phrase))

((Author(s), Corresponding Author(s)*))
_____ **Page – Page**

((Title Text))

((TOC Graphic))

((Text for Table of Contents, max. 450 characters))

Submitted to *Angew. Chem. Int. Ed.*, November 2013

SUPPORTING INFORMATION

Nano-sized Au@Prussian Blue Analogues Heterostructures: Towards Multifunctionality at the Nanoscale.

Guillaume Maurin-Pasturel,[a] Jêrome Long,[a] Yannick Guari,[a]* Christian Guerin,[a] Franck Godiard,[b]

Marc-Georg Willinger[c] and Joulia Larionova.[a]

[a] Institut Charles Gerhardt, UMR 5253, Chimie Moléculaire et Organisation du Solide, Université Montpellier II, Place E. Bataillon, 34095 Montpellier cedex 5, France.
[b] Service de microscopie électronique, Université Montpellier 2, Place Eugène Bataillon, 34095 Montpellier Cedex 5, France.
[c] Fritz Haber Institute of the Max Planck Society, Department of Inorganic Chemistry, Faradayweg 4-6, D-14195 Berlin, Germany.

Experimental Section

Syntheses

Materials: All chemical reagents were purchased and used without further purification: potassium ferricyanide ($K_3[Fe(CN)_6]$) (Acros Organics, 99%), gold(I) potassium cyanide ($K[Au(CN)_2]$) (Alfa Aesar, 99.99 %), potassium hexacyanochromate(III) ($K_3[Cr(N)_6]$) (Aldrich, 99.99 %), Nickel(II) chloride hexahydrate ($NiCl_2{\cdot}6H_2O$) (Chimica, 99 %), potassium borohydride (KBH_4) (Acros Organics, 98 %), potassium cyanide (KCN) (Acros Organics, 97 %), ultra pure water.

Au core NPs: In a typical experiment, KBH_4 (0.63 mmol) was added to 100 mL of an aqueous solution of $K[Au(CN)_2]$ (4.8×10^{-5} mol, 4.8×10^{-4} M) under vigorous stirring at 25°C. The colorless solution rapidly turned red, indicating the formation of NPs. After 20 min, they were used immediately in the next step.

Single layered Au@KNiFe core@shell NPs: 10 mL of an aqueous solution of $K_3[Fe(CN)_6]$ (5.65 mM) and 10 mL of an aqueous solution of $NiCl_2{\cdot}6H_2O$ (5.00 mM) were simultaneously added (2 mL/h) to the gold NPs solution under vigorous stirring at 25°C. After completion of the addition, the solution was vigorously stirred for one hour. The aqueous solution of NPs was centrifugated at 20000 rpm during 15 mins. The supernatant was removed and the NPs were washed with water and centrifugated again at 20000 rpm during 15 mins. The supernatant was removed and the NPs were washed with ethanol and centrifugated at 20000 rpm during 10 min and were dried under vacuum.
Purple powder. IR (KBr): ν_{CN} = 2094 cm^{-1} (Fe^{II}-CN-Ni^{II}). Anal. Found: Au, 41.3 : K, 9.11 ; Ni, 11.4 ; Fe, 8.67 ; C, 11.2 ; N, 13.1.

Hollow KNi[Fe(CN)$_6$] NPs: 5 mg of Au@KNiFe NPs were added to 10 mL of an aqueous solution of KCN (10^{-3} M) under vigorous stirring for 24h. The suspension, initially purple, becomes progressively colorless.
White powder. IR (KBr): ν_{CN} = 2091 cm^{-1} (Fe^{II}-CN-Ni^{II}).

Double layered Au@KNiFe@KNiCr core@shell NPs: 10 mL of an aqueous solution of $K_3[Cr(CN)_6]$ (5.65 mM) and 10 mL of an aqueous solution of $NiCl_2 \cdot 6H_2O$ (5.0 mM) were simultaneously added (2mL/h) to 50 mL of an aqueous solution of Au@KNi[Fe(CN)$_6$] core@shell NPs (10 mg in 50 mL) under vigorous stirring at 25°C. After completion of the addition, the solution was stirred for one hour.
Au@KNiFe@KNiCr: Mauve powder. IR (KBr): ν_{CN} = 2172 (Cr^{III}-CN-Ni^{II}), ν_{CN} = 2094 (Fe^{II}-CN-Ni^{II}) cm^{-1}. Anal. Found: Au, 8.45 : K, 3.69 ; Ni, 26.2 ; Fe, 3.59 ; Cr, 12.0 ; C, 21.3 ; N, 24.9.

Physical Characterization

Infrared spectra were recorded as KBr disks on a Nicolet Model 510P spctrophotometer. UV-Vis spectrums were collected on a Specord 210 spectrophotometer. Transmission Electron Microscopy (TEM) observations were carried out at 100 kV (JEOL 1200 EXII). NPs' size distribution histograms were determined using enlarged TEM micrographs taken at magnification of 100K on a statistical sample of ca. 300 NPs. HRTEM measurements were performed on a JEOL 2200FS and a Magnetic susceptibility data were collected with a Quantum Design MPMS-XL SQUID magnetometer working in the temperature range 1.8 – 350 K and up to 7 T.

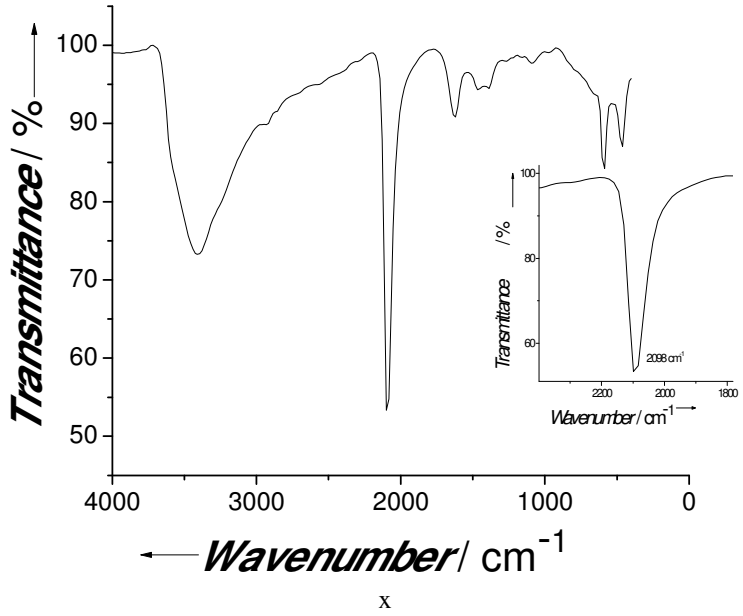

x

Figure 1S. IR spectrum of Au@KNiFe NPs. The inset shows the cyanide stretching region.

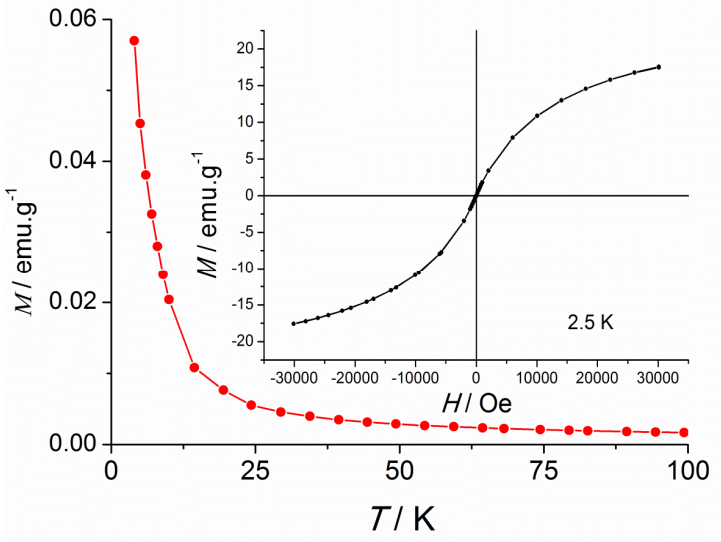

Figure 2S. Magnetization vs. temperature curve performed for Au@KNiFe NPs with an applied field of 50 Oe. Inset: hysteresis loop performed at 2.5 K.

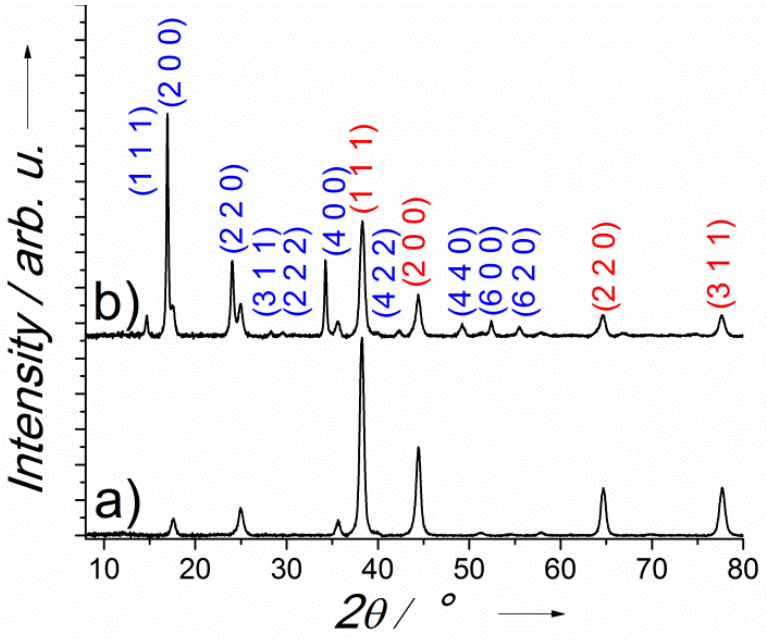

Figure 3S. Room temperature PXRD pattern for Au@KNiFe (a) and Au@KNiFe@KNiCr; (b) The red (h k l) are related to the gold phase while the blue (h k l) accounts for the Prussian Blue analogues.

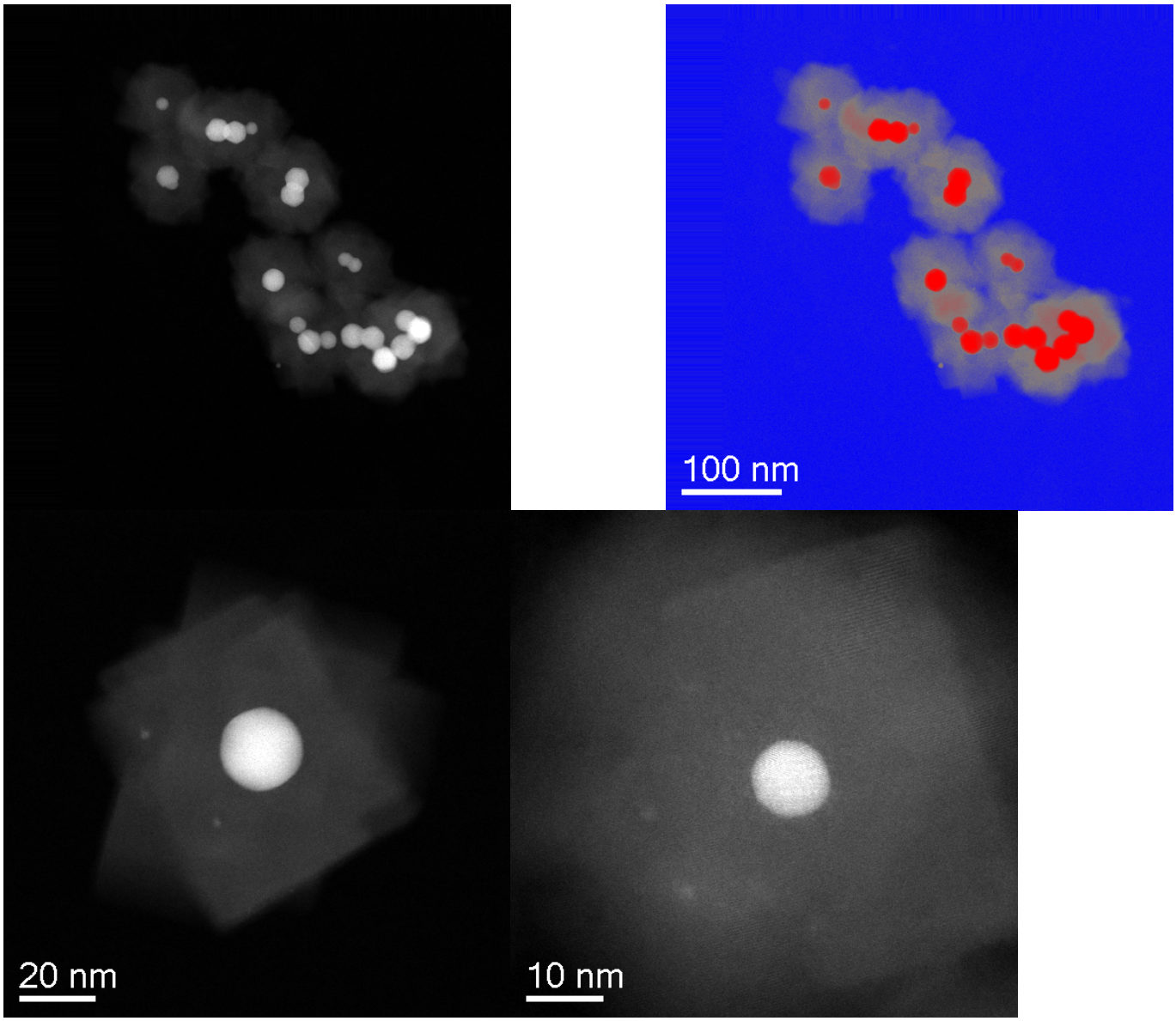

Figure 4S. Scanning Transmission Electronic Microscopy – High Angle Annular Dark field (STEM-HAADF) images of a collection of core@shell Au@KNiFe NPs (Up) and an individual one (Down).

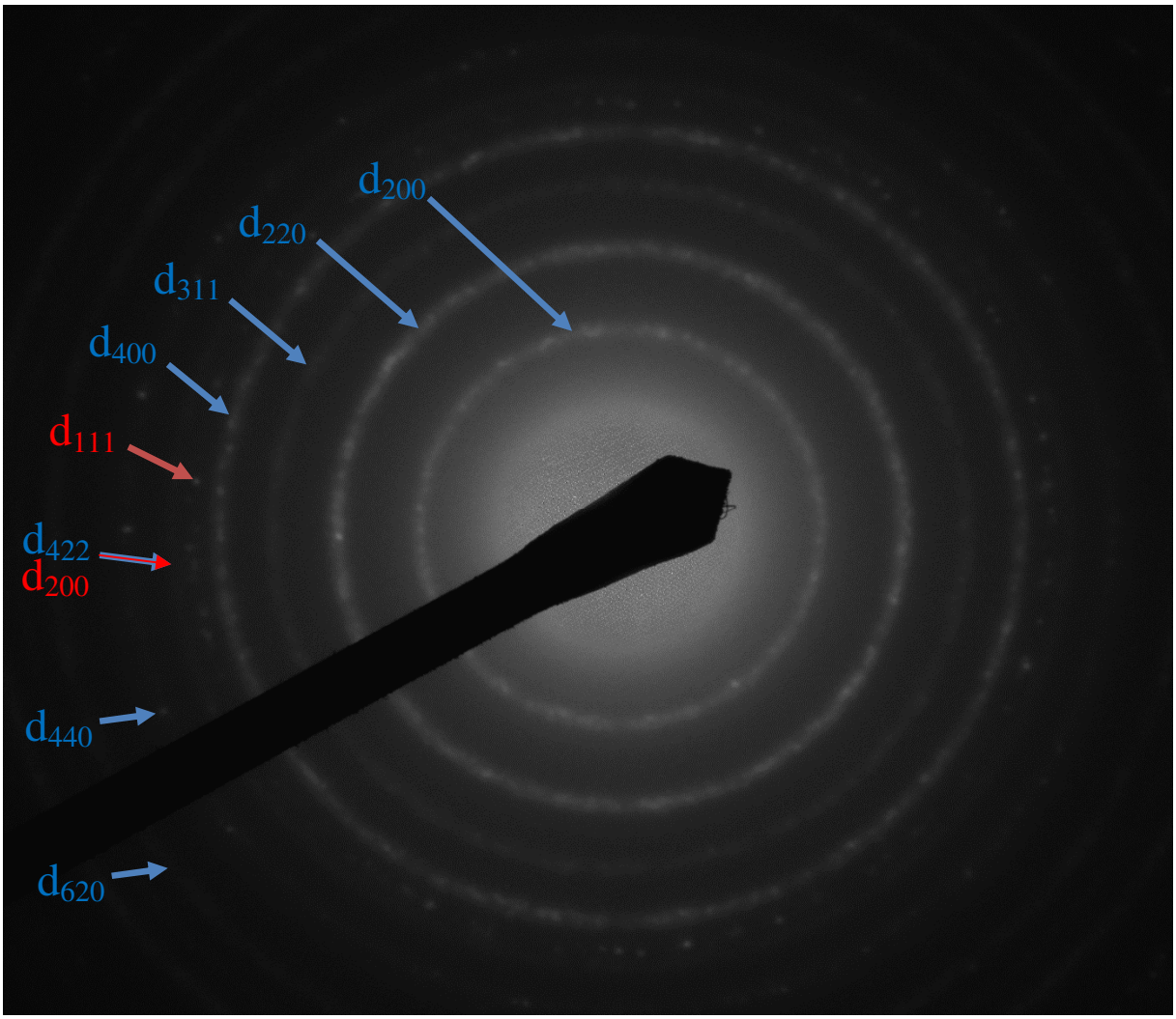

Figure 5S. Single Area Electron Diffraction (SAED) on an individual core@shell Au@KNiFe NPs with corresponding d_{hkl} in red for the gold core and d_{hkl} in blue for the $Ni^{II}_2[Fe^{II}(CN)_6]$ shell.

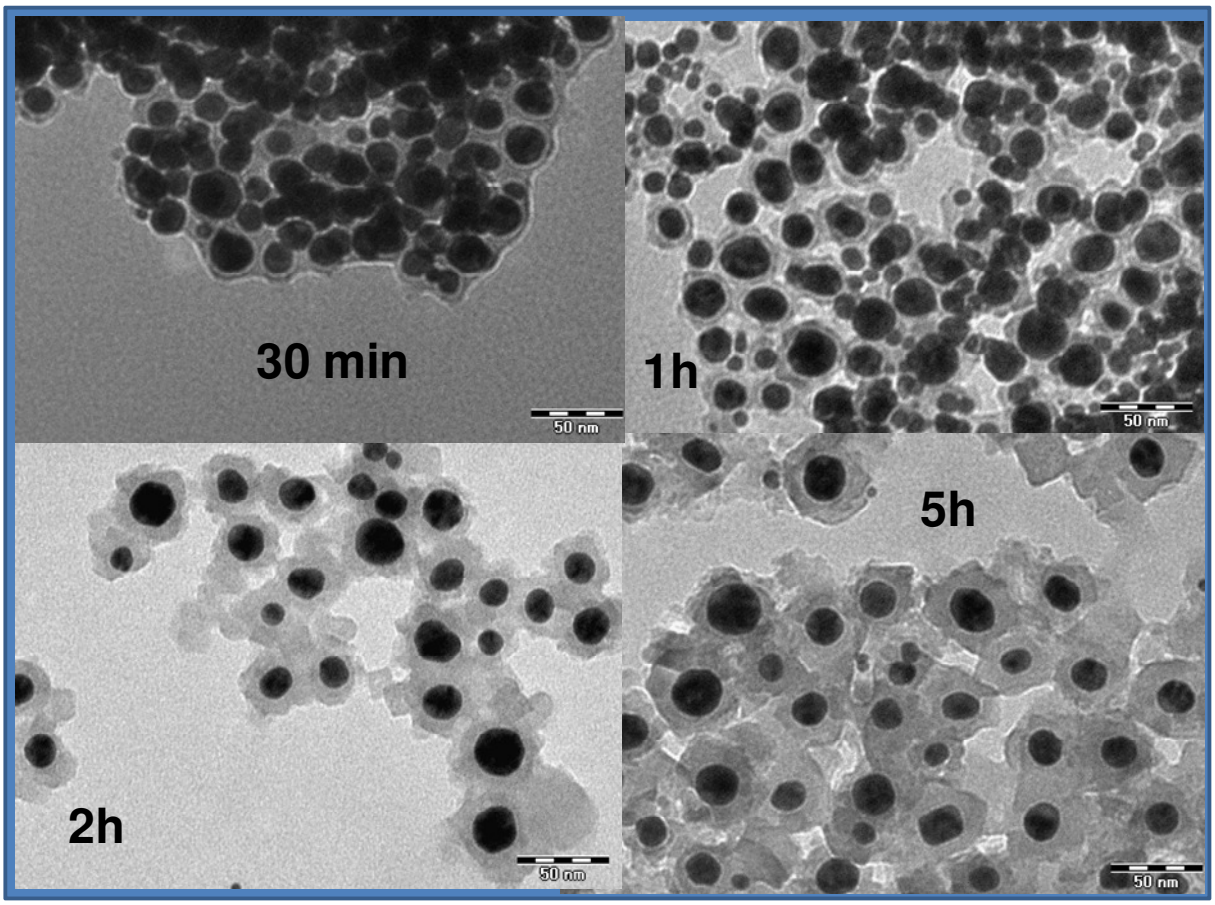

Figure 6S. TEM images of $K_{1.20}Ni^{II}[Fe^{II}(CN)_6]_{0.80}$ shell growth followed in times for Au@KNiFe NPs.

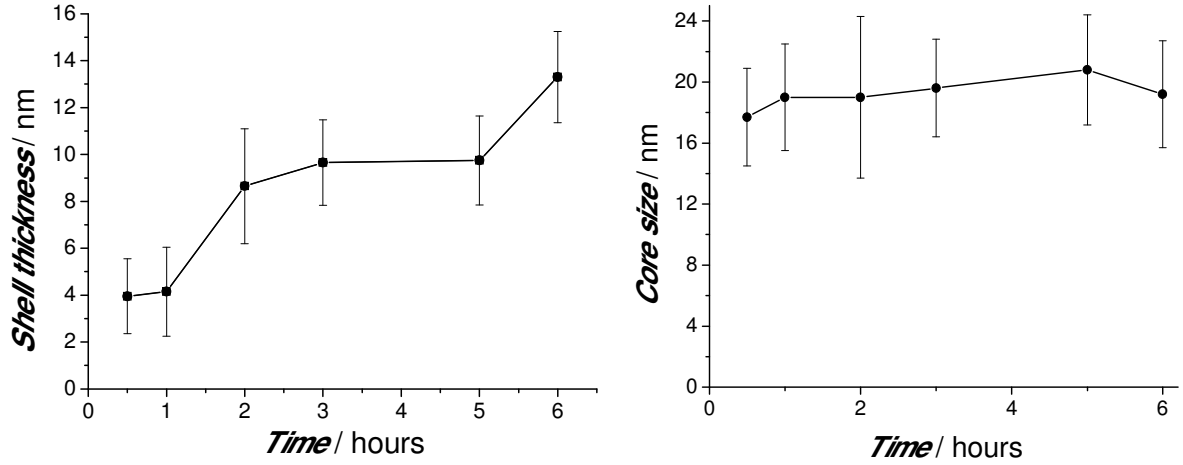

Figure 7S. Left: $K_{1.20}Ni^{II}[Fe^{II}(CN)_6]_{0.80}$ shell thickness dependence as a function of reaction time for Au@KNiFe NPs. Right: Au core size dependence as a function of reaction time for Au@KNiFe

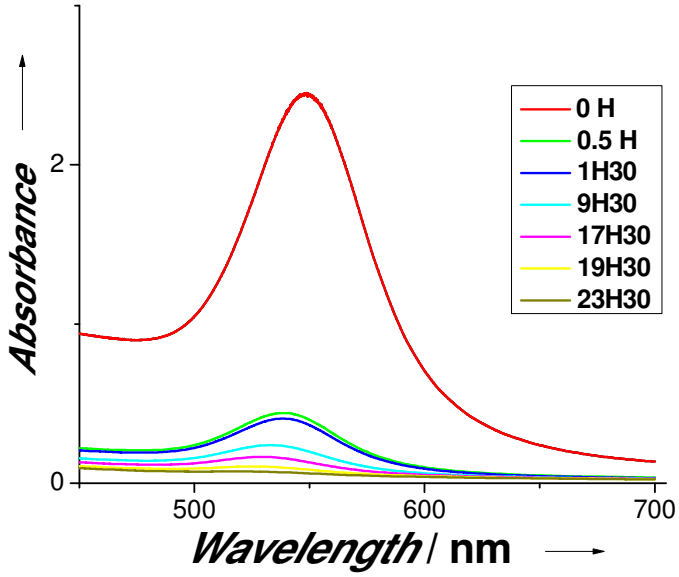

Figure 8S. Electronic spectra in the visible region performed for follow the etching reaction for Au@KNiFe NPs.

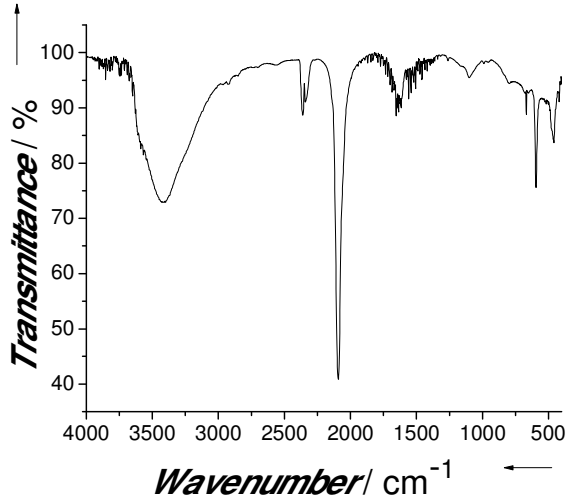

Figure 9S. IR of hollow $KNi[Fe(CN)_6]$ NPs.

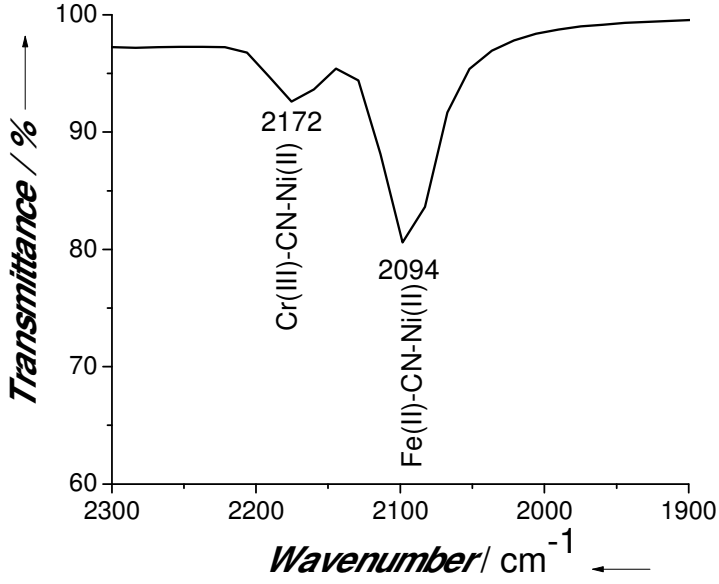

Figure 10S. IR spectra (cyanide region) of double layered Au@KNiFe@KNiCr NPs.

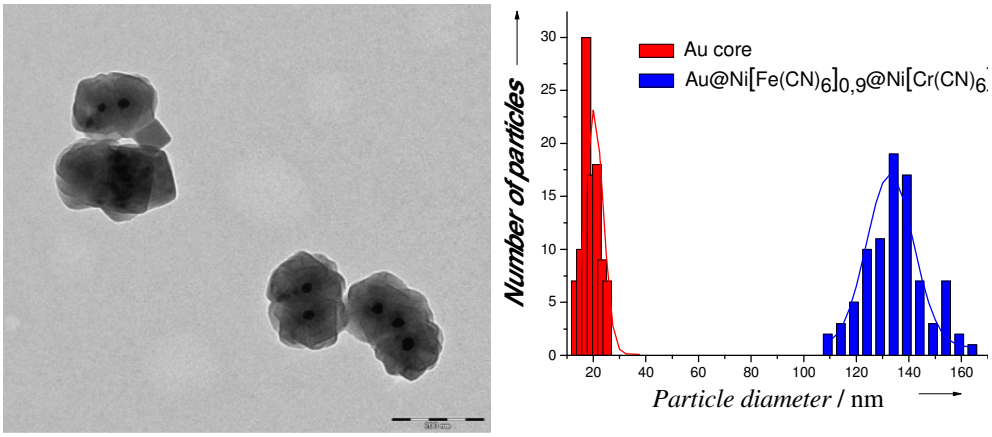

Figure 11S. Left: TEM image of the Au@KNiFe@KNiCr NPs ; right) the corresponding histograms of the size distribution for the gold core (red) and the total size (blue).